ROBUST LAPLACIAN REGULARIZATION FOR ENHANCED IMAGE RECONSTRUCTION

Guoping Qiu

School of Computer Science, The University of Nottingham, United Kingdom

ABSTRACT

This paper presents a new robust regularization approach to the reconstruction of enhanced images from noisy observations. A new regularization constraint designed explicitly to boost non-noise fine image details is optimized together with a traditional two-term (smooth and fidelity) regularization functional. A gradient descent based numerical solution is developed which is shown to be numerically stable and converge within finite iterations. Experimental results are presented to demonstrate that images constructed by the new method contain much better preserved edges and fine details.

1. INTRODUCTION

Estimating the underlying scenes from observed noisy data is an important inverse problem in image processing. Generally speaking, this is an ill-posed inverse problem. One way to solve the problem is to use regularization theory [2, 3] and obtain a solution by minimizing a cost function of the form of (1)

$$E(f) = \int_{\Omega} (f(x) - d(x))^2 dx + l \int_{\Omega} j(\nabla f(x)) dx \qquad (1)$$

where $\nabla f(x)$ is the gradient of $f(x)$, j is an edge preserving nonlinear function, Ω denotes the image domain, and λ is a regularization factor which balances the influences between the two terms of (1).

The first term of (1) measures the fidelity of the estimation and the second term measures the smoothness of the reconstruction. The regularization parameter is chosen such that the recovered original image is faithful to the observed data and at the same time it is smooth. The choice of an appropriate edge preserving function j is very important which should encourage smoothing within regions and discourage smoothing across region boundaries. A number of different functions have been used in the literature. The authors in [1] explored several possible choices of j in the context of anisotropic diffusion filtering and robust estimation. Other possibilities of j include those suggested in the original nonlinear anisotropic diffusion model of Perona and Malik [5]. The Tukey's biweight function was found to give better performance than the Perona-Malik's Lorentzian function. Tukey biweight function is defined as (2) and its first order derivative defined as (3).

One of the problems with the functional of (1) is that it can still smear image details and cause the recovered images to be blurred. This is illustrated in Fig. 1 where the borders between piecewise constant regions have been smeared by the regularization method of (1) (see Fig. 1 (c)) and edge detection has failed to recover the region borders from the restored image (see Fig. 1 (f)). Please see text in Section 4 for details of the experimental procedures.

$$j(x,s) = \begin{cases} \frac{x^2}{s^2} - \frac{x^4}{s^4} + \frac{x^6}{3s^6} & \text{if } |x| \le s \\ \frac{1}{3} & \text{Otherwise} \end{cases} \qquad (2)$$

$$j'(x,s) = \begin{cases} x\left[1 - \left(\frac{x}{s}\right)^2\right]^2 & \text{if } |x| \le s \\ 0 & \text{otherwise} \end{cases} \qquad (3)$$

One solution to overcome this problem is to introduce line process [2], best known as the Mumford-Shah functional [4]:

$$E(f,K) = \int_{\Omega} (f(x) - d(x))^2 dx + l \int_{\Omega - K} j(\nabla f(x)) dx + a|K| \qquad (4)$$

where K is the (closed) set of edges and the last term of (4) is the penalty for introducing the line segments. In the literature, there have been many modifications to this general scheme. However, numerical solution to (4) is nontrivial.

In this paper, we introduce a new regularization constraint to the standard functional of (1). This new constraint explicitly boosts edges and details thus preventing excessive blurring.

2. LAPLACIAN REGULARIZATION

Our new functional has the form of (5)

$$E(f) = l_1 \int_{\Omega} (f(x) - d(x))^2 dx + l_2 \int_{\Omega} j(\nabla f(x)) dx + l_3 \int_{\Omega} x(f(x) - f(x) * h(x)) dx \qquad (5)$$

where, λ_1, λ_2 and λ_3 are non-negative weighting constants, $h(x)$ is the systems point spread function (PSF), x is a nonlinear function similar to j and * denotes spatial domain convolution. The first two terms are the same as in (1), the third term is the new Laplacian regularization constraint. The interpretation of the first two terms is similar to that in (1). We explain the purpose of the third term.

For analysis convenience, we first set $x(x) = x$ and re-write the third term of (5) as

$$E_L(f) = \int_{\Omega} \left(f(x) - f(x) * h(x) \right) dx \qquad (6)$$

In order to understand the effects of minimizing (6), lets assume that the function $f(x)$ and the point spread function $h(x)$ both take the form of a Gaussian:

$$f(x) = \frac{1}{s_f \sqrt{2p}} \exp\left(-\frac{x^2}{2s_f^2} \right) \qquad (7)$$

$$h(x) = \frac{1}{s_h \sqrt{2p}} \exp\left(-\frac{x^2}{2s_h^2} \right) \qquad (8)$$

(6) now becomes

$$E_L(s_h, s_f) = \qquad (9)$$
$$\frac{1}{\sqrt{2p}} \int_{\Omega} \left(\frac{1}{s_f} \exp\left(-\frac{x^2}{2s_f^2} \right) - \frac{1}{\sqrt{s_f^2 + s_h^2}} \exp\left(-\frac{x^2}{2(s_f^2 + s_h^2)} \right) \right) dx$$

Clearly, E_L is a function of the widths of $f(x)$ and $h(x)$, σ_f and σ_h . Fig. 2 (a) plots E_L as a function of the ratio of the width of f and h and Fig. 2 (b) plots the first order derivative of E_L with respect to the signal width of $f(x)$. Depending on this ratio value, we can observe following interesting points: For signal features that are much narrower than the PSF, E_L is very large and such signal (noise) will be considered as outliers by ξ. For signal feature that is narrower than the PSF, expanding its width will reduce E_L rapidly and it reaches its minimum at about $\sigma_f = 1.5\sigma_h$. For signal feature that is much wider than the PSF, E_L is small and it changes very slowly with σ_f. Therefore, a rough explanation of the effect of minimizing E_L is (1) the process will leave large homogenous regions unchanged, (2) it will expand non-noise detail features to roughly the width of the PSF, and (3) it will treat very sharp changes as outliers. We will see in the experiment section that such a process together with the other two terms in (5) will enable the reconstruction process to preserve edges and sharp features better.

3. NUMERICAL SOLUTION

For notation convenience, we use 1-D signal to illustrate the solution to the problem. There are various possibilities to find a solution to (5), here we will use a gradient descent approach to solving the equation. The discrete formulation of (5) can be written as

$$E(f) = l_1 \sum_x [f(x) - d(x)]^2 + l_2 \sum_x \sum_i j[f(x) - f(x+i)] \qquad (10)$$
$$+ l_3 \sum_x x[(f(x) - \sum_k f(x+k)h(k))]$$

The partial derivative of E with respect to f can now be derived:

$$\left. \frac{\partial E}{\partial f} \right|_x = 2l_1 (f(x) - d(x)) + l_2 \sum_i j'(f(x) - f(x+i)) + \qquad (11)$$
$$l_3 \left(- \sum_{\forall k, k \neq 0} h(k) x'(L(x+k)) \right)$$

where

$$L(x) = f(x) - \sum_k f(x+k)h(k) \qquad (12)$$

and $j'(x)$ and $x'(x)$ are the first order derivatives of $j(x)$ and $x(x)$ respectively.

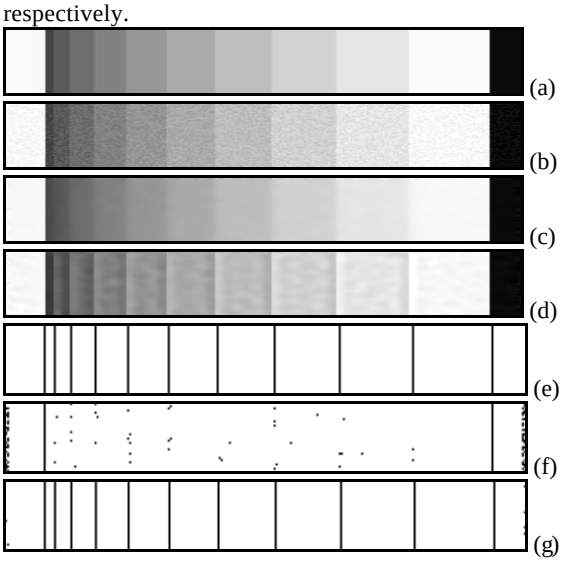

Fig. 1, (a) Synthetical stripes image, the intensity in each vertical stripe is a constant. (b) Noise corrupted image of (a). (c) Restored from (b) using (1). (d) Restored from (b) using (5). (e) Stripes borders of the original (a). (f) Stripe borders from (c) via edge detection. (g) Stripe borders from (d) via edge detection.

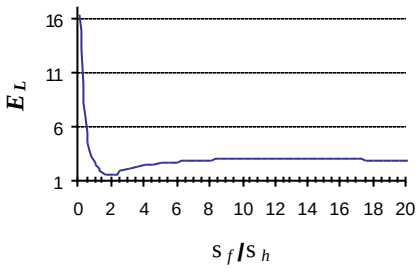

(a)

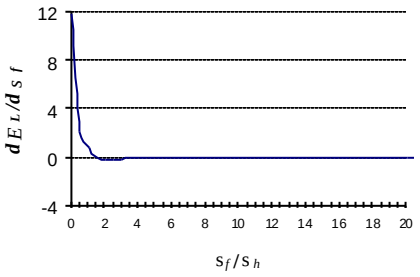

(b)

Fig. 2 The Laplacian regularizer as a function of the widths of the signal and the point spread function.

Once the partial derivative is computed, then gradient descent technique can be used to iteratively recover the original image $f(x)$. This process can be written as

$$f_{t+1}(x) = f_t(x) - h\frac{\partial E}{\partial f}\bigg|_{f=f_t(x)} \qquad (13)$$

where $0 < \eta < 1$ is the updating step-size and t denotes the iterating sequential index. In the next section, we report experimental results of the new method.

4. EXPERIMENTAL RESULTS

We have performed various experiments to evaluate the usefulness of the new image reconstruction functional. In the experiments, we choose the Tukey biweight function (2) for both the edge preserving potential function j and for the Laplacian non-linear regularization function x. and we use a Gaussian with a $\sigma_h = 1$ pixel as the point spread function $h(x)$.

To choose an appropriate scale parameter σ for the biweight functions, we use a robust estimation method similar to that proposed in [1] and select the scale according to

$$s = 3.3MAD = 3.3Median\{|I - Median\{I\}|\} \qquad (14)$$

where MAD denotes the median absolute deviation, Median $\{I\}$ is the median value of the set $\{I\}$. In the case of the edge preserving function j, the set $\{I\}$ is obtained from $\{I\} = \{2f(x) - f(x\text{-}1) - f(x\text{+}1)\}$. In the case of Laplacian regularization function ξ, the set $\{I\} = \{L(x)\}$.

The choice of the regularization parameters λ_1, λ_2 and λ_3 is done empirically. This is the approach used by almost all authors. Although a systematical method is desirable, this has proven to be difficult. Fortunately, we found that the scheme is not overly sensitive to the choices of these parameters. In all our experiments, we were able to find a "good" set of parameters for a given image after a few tries. A rough heuristic is this: λ_1 is related to the signal to noise ratio (SNR). If SNR is small, then λ_1 should be small and λ_2 should be relative large so that the smooth term is sufficiently large to regularize the image. After determining the values of λ_1 and λ_2, we fix them and choose the value of λ_3 by first setting it to a small value and then gradually increase it until a satisfactory value is found.

Apart from the regularization parameters, the updating step-size is also selected by experiment. There have been many studies in the neural network literature on how to choose such parameters, e.g., [6], but this is beyond the scope of this paper. We found that setting $\eta = 0.25$ works very well for all our experiments.

Fig. 3 shows the result of reconstructing a noise corrupted synthetical piecewise constant image. It is seen that by introducing the new term, we were able to restore the edge features much better. The new method is numerically stable and for this image the algorithm converged at about 500 iterations and further iterations did not change the result. In this Figure it is seen that the reconstructed image after 2000 iterations is almost the same as that after 500 iterations.

Fig. 4 shows the result of reconstructing a noisy MRI image. Again, it is seen that with the introduction of the new Laplacian regularization term, we were able to restore sharp and finer details of the image. It is again seen that the algorithm is numerically stable. For this image, again, the reconstruction hardly changed by further iterations after 500 updates.

5. CONCLUDING REMARKS

In this paper, we have presented a new regularization constraint which, when optimized together with the traditional regularization functionals, enables the reconstruction of enhanced images from noisy observations. We have also presented a numerical solution and shown that the new algorithm is numerically stable.

6. REFERENCES

1. M. J. Black, G. Sapiro and D. Marimont, "Robust anisotropic diffusion", IEEE Trans. On Image Processing, vol. 7, pp. 421 – 432, 1988
2. C. Koch, J. Marroquin and A. Yuille, "Analog neuronal networks in early vision", Proc. Natl. Acad. Sci. USA, vol. 83, pp. 4263 – 4267, 1986
3. O. Scherzer and J. Weickert, "Relations between regularization and diffusion filtering", Journal of Mathematical Imaging and Vision, vol. 12, pp. 43 – 63, 2000
4. D. Mumford and J. Shah, "Optimal approximations by piecewise smooth functions and associated variational problems", Communications in Pure and Applied Mathematics, vol. 42, no. 4, 1989
5. P. Perona and J. Malik, "Scale space and edge detection using anisotropic diffusion", IEEE Tran. PAMI, vol. 12, pp. 629-639, 1990
6. S. Haykin, Neural Network: A comprehensive foundation, 2nd Edition, Prentice Hall International, 1999

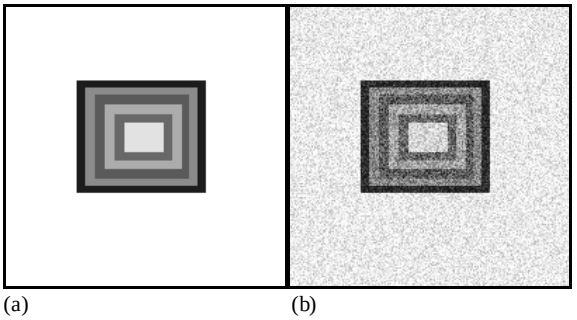

(a) (b)

Fig. 3 Experimental results on a synthetical image. (a) original. (b) noise corrupted image. (Contd.)

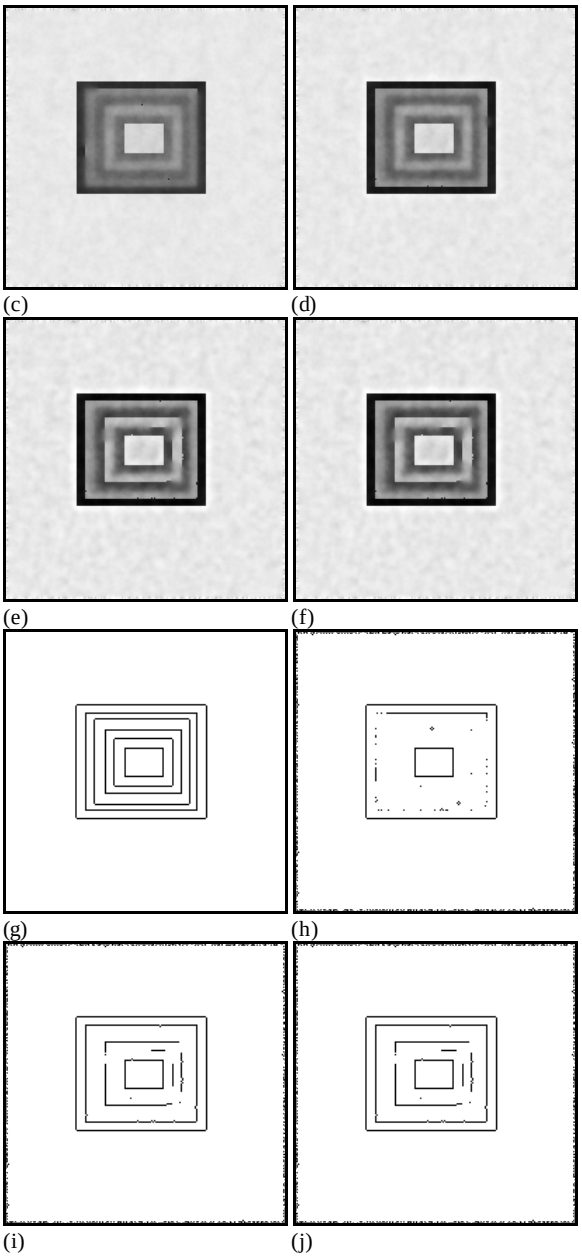

Fig. 3 Experimental results on a synthetical image. (a) original. (b) noise corrupted image. (c) reconstructed image λ_1 =0.1, λ_2 = 1, λ_3 = 0 (without Laplacian regularization). (d) reconstructed image λ_1 =0.1, λ_2 = 1, λ_3 = 0.5. (e) reconstructed image λ_1 =0.1, λ_2 = 1, λ_3 = 1. (c) (d) (e) are results after 500 iterations. (f) reconstructed image λ_1 =0.1, λ_2 = 1, λ_3 = 1, after 2000 iterations. (g) region borders of the original image. (h) region borders based on edge detection from (c). (i) region borders based on edge detection from (e). (j) region borders based on edge detection from (f).

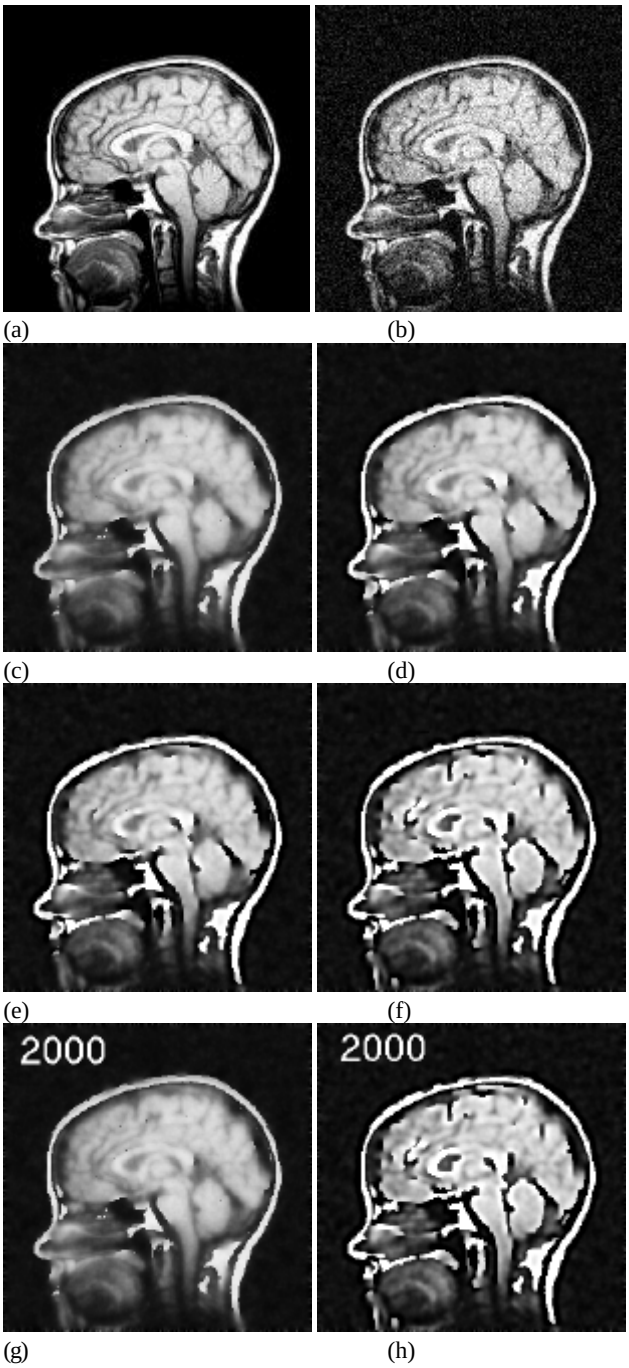

Fig. 4 Experimental results on a MRI image. (a) original. (b) noise corrupted image. (c) reconstructed image λ_1 =0.1, λ_2 = 1, λ_3 = 0 (without Laplacian regularization). (d) reconstructed image λ_1 =0.1, λ_2 = 1, λ_3 = 0.5. (e) reconstructed image λ_1 =0.1, λ_2 = 1, λ_3 = 0.7. (f) reconstructed image λ_1 =0.1, λ_2 = 1, λ_3 = 1. (c) (d) (e) and (f) are results after 500 iterations. (g) reconstructed image λ_1 =0.1, λ_2 = 1, λ_3 =0 after 2000 iteration. (h) reconstructed image λ_1 =0.1, λ_2 = 1, λ_3 = 1 after 2000 iterations.